Revised Manuscript clean and final version

Click here to view linked References

Unveiling stimulation fluid-driven alterations in shale pore architecture through combined interpretation of TD-NMR and multi-component gas adsorption

Bryan X. Medina-Rodriguez[a], Vladimir Alvarado[a,*], Matthew Edgin[b], John Kaszuba[b,c]

[a] *Department of Chemical Engineering, University of Wyoming, Laramie, Wyoming, 82071*
[b] *Department of Geology & Geophysics, University of Wyoming, Laramie, Wyoming, 82071*
[c] *School of Energy Resources, University of Wyoming, Laramie, Wyoming, 82071*

Abstract

The hydraulic fracturing stimulation process can alter petrophysical and flow properties of the shale matrix in unconventional reservoirs. These alterations can result from interactions with native and exogenous fluids, and can be detrimental to reservoir productivity. Different experimental procedures have been proposed to study reactive processes and thereby understand the aforementioned interactions. Most published works do not consider the rock initial saturation with formation fluid, or the effect of organic matter (OM). To gain insights into these effects, two reactive experimental sets, differing in experimental conditions, were conducted. In the first set, at 125°C and 45 MPa, a stimulation fluid surrogate was put in contact with Baxter Shale samples, previously saturated and equilibrated with synthetic formation fluid. A baseline consisted of exposure to formation fluid exclusively. In the second set, at 0.08 MPa and 25°C, contact with stimulation fluid took place as in the first set. Two additional assays in this second set either skipped the initial formation fluid saturation or removed the OM, respectively. Petrophysical properties analyses, focused on the pore architecture, relied on the combined interpretation of gas adsorption and Time-Domain Nuclear Magnetic Resonance (TD-NMR). Results show that the presence of the formation fluid significantly restricts pore space accessibility

*Corresponding author

to the stimulation fluid and mitigates the pore-architecture alteration to the macro-pore region. Mineral dissolution and precipitation dominate over surface or wettability alteration. Next, results suggest that the OM restricts accessibility to some pores. Ultimately, the equilibration process with synthetic formation fluid drives mainly surface alteration, unhindered by OM.

Keywords: `Fracking`, Pore Architecture, Shale Reactivity, Organic Matter, NMR, Gas Adsorption

---

1. Introduction

Production of unconventional reservoirs has driven Oil and Gas activity in the past two decades, leading to significant research efforts in the field. These efforts have aimed at developing economically viable exploitation plans for these reservoirs [1–3]. However, the aim remains almost insurmountable due to the complexity of this type of reservoir, namely the poor understanding of mass transport in the tight rock matrix and the permeability span from the nano- to milli-darcy values. For industry, hydraulic fracturing, also colloquially known as fracking, appears to be the most common and cost-effective technique to commercially produce hydrocarbons from unconventional reservoirs. The key feature of this stimulation technique is the creation of permeable channels or the re-opening of those naturally existing pathways to fluid flow [4–8].

The process of hydraulic fracturing involves the use of complex fluids of a gamut of salinities, pH and content of additives. Each component in the fluid is required to address operational constraints and reservoir characteristics [9, 10]. Fracking has been shown, however, to induce some detrimental side effects that can be observed in the short term, e.g. unexplained low recovery of flowback water after an injection step [11]. Other side effects in the long term include the decline in production rates [12, 13] and contamination of sources of potable water [14, 15].

Such problems are often intertwined and usually the result of interactions between the injected fluid and the pristine reservoir components, i.e. the rock ma-

trix, hydrocarbons and formation water. The interactions that induce changes in the rock properties occur through multiple mechanisms. In several research works, mineral precipitation and dissolution have been identified as the driving mechanisms for petrophysical properties alteration, namely changes in porosity and permeability, and micro-fracture development [16–20]. Other mechanisms such as gravity segregation, changes in capillarity [21, 22], chemical osmosis or mineral hydration [11, 23] have also been proposed. Whenever the aforementioned mechanisms can cause pore blockage, changes in fluid flow channels may occur. Other authors point to wettability alteration as a precursor to adverse scenarios, for which Organic Matter (OM) alteration and adsorption effects appear to play the most significant roles in alteration of the rock capillarity signature [24–28]. In the end, changes in the rock matrix appear to result from a combination of several mechanisms.

A variety of experiments has been performed to emulate the fracturing process in the laboratory and thereby infer phenomena occurring in the reservoir [11, 16, 17, 29, 30]. While the goal is to understand rock changes, experimental protocols differ in sample preparation and experimental conditions, but in most cases the protocols do not adequately represent the reservoir system. In addition, the variety of technologies used to analyze changes, especially in the rock matrix, challenges the selection of the most cost-effective technique to collect information [31]. Even when a good protocol is at hand, gathering the necessary information might not be possible. The challenges are the degree of heterogeneities, the singular characteristics of unconventional reservoirs around the world and the multi-scale nature of the pore architecture. We define pore architecture as a unique, identifiable pore space composite in the rock matrix that encompasses micro, meso and macropores of different geometries, sizes, and shapes, along with topology (connectivity) across the hierarchy of pore spaces.

Structural and wettability changes are often studied separately, and most results in the literature highlight that changes are more likely to affect the structure of the rock, generally micro-fractures, and fractures networks [32, 33]. Even if the effects extend to micro- and meso-pores or to surface properties, the

conclusion could be misguided, since in most cases not all reservoir components are considered. In most experimental designs, the stimulation fluid is in direct contact with the rock matrix, without considering the presence and equilibration of the rock with the connate formation fluid [10].

Edgin et al. [34], Edgin [35] found evidence of geochemical effects of the fracturing fluid after injection during the stimulation process throughout the performance of a set of reactive experiments at reservoir conditions (45 MPa and 125^oC). The novelty of his experimental procedure included a first step of saturation and equilibration of the rock with synthetic formation fluid. This procedure provided a baseline and better represented conditions akin to those of the real reservoir system, differing from other studies in the lack of forced fluid displacement and conditions for which capillary forces and diffusion were dominant transport driving mechanisms. Edgin et al. [34], Edgin [35] results evidenced geochemical alteration of the rock specimens after contact with formation fluid and after the injection of the stimulation fluid under more realistic conditions. The author identified geochemical changes that were associated to changes in the pore-architecture, dominantly in the macropore region, apparently leaving the micro- and mesopores region mostly unaltered. Edgin's work left unanswered questions regarding the connection between pore architectural changes and possible rock-surface alteration, the impact of the presence of formation fluid and role of the different components, such as the organic matter, had during the reaction process.

The main purpose of the study herein is threefold. First, we would like to test the hypothesis that pore architectural changes, under Edgin's experimental conditions, correspond dominantly to pore structural modification rather than surface alteration. Second, we hypothesize that organic matter distribution in the matrix bars accessibility to meso and micropores in this type of rock. Finally, we aimed at determining the feasibility of conducting hypotheses testing via the combined use of gas adsorption isotherm and time-domain nuclear magnetic resonance. Gas adsorption is able to yield semi-quantitative information regarding changes in the surface area and pore structure, especially in regards to

the micro and mesopores. Due to their distinct interactions with rock surfaces, the use of different gasses, i.e. N_2, CO_2 and CH_4, can provide information regarding shale alteration. N_2 and CO_2 are often used to analyze structural changes [36–42] , whereas CH_4 has a closer relationship with wettability. Other authors have shown that a change on the wettability of shales can have a higher impact on the adsorption in comparison with any other changes taking place [43] and the magnitude of the impact is related as well to the mineral composition [24]. The application of NMR, on the other hand, has served as a useful complementary technique from which we have been able to obtain a better and simpler representation of the process affecting the rock matrix [18, 44–46].

To test the aforementioned hypotheses, Baxter Shale samples from two sets of experiments with similar characteristics are analyzed. Samples at reservoir conditions were obtained from the experiments performed by Edgin et al. [34], Edgin [35]. Other samples were subject to experiments at milder experimental conditions, labeled here as laboratory conditions. These experiments were performed to further explore the role of the formation fluid and the OM during the interaction with stimulation fluid. In addition, experiments with glass-bead packs were conducted under some of the same conditions used for shale samples and characterized via TD-NMR, to shed light on surface processes or wettability alteration. These observations served to interpret shale results through analogy with detected shifts in T_2 peaks in beads tests.

Results in this work unveiled how the OM distribution and the presence of formation fluid affected rock alteration driven by the stimulation. First, the formation fluid constrained the stimulation fluid access to the meso- and micro-pores. This effect translated into a diminished surface and pore structure alteration. Second, the OM distribution barred accessibility to a section of the pore architecture and appeared to play a minimum role in reactions, including the interaction with the synthetic formation fluid that predominantly induced surface alteration.

2. Materials

2.1. Baxter Shale

Rock specimens used in this study correspond to samples of the Baxter Shale from the Greater Green River Basin in Wyoming. The Green River Basin has been the source for hydrocarbon in the last five decades, and the Baxter Shale, since 2007, has shown to be an important source for gas production. This shale possesses lithological characteristics found in successful unconventional gas plays [34, 35, 47]. The Baxter Shale samples were obtained from the Canyon Creek N^o 41 well in the Canyon Creek Field, and are predominantly composed of quartz (34 wt%), calcite (26 wt%) and clay (23 wt%) with smaller amounts of dolomite, plagioclase, pyrite, and K-Feldspar. The total organic content (TOC) is 2.05 wt% and the thermal maturity correspond to vitrinite reflectance of 1.4. The bulk density is 2.35 g/cm3.

2.2. Glass beads

In addition to the rock samples, borosilicate glass beads 425-600 μm in diameter from Sigma-Aldrich were used to qualitatively assess the ability of the two fluids to induce surface or wettability alteration. A group of glass beads was treated with a solution of 5% dimethyldichlorosilane in toluene to alter their initial surface properties/wettability [48]. Glass beads that underwent this process are identified as Oil-Wet (OW), meanwhile those that were not treated are identified as Water-Wet (WW).

2.3. Formation and stimulation fluid

Formation and stimulation fluids used in the experiments were synthesized in the laboratory as per Edgin et al. [34], Edgin [35]. Properties of the fluid as ion concentration, pH, redox potential (Eh) and Charge Balance Error percentage (C.B.E. %) are presented in Table 1. The synthesized formation fluid is consistent with formation fluid produced from the Baxter Shale. The stimulation fluid used in the experiments correspond to an acidic fluid and its composition was determined considering Green River water as the make-up fluid [49] and additives

as determined from completion reports from a public database [50]. Important additives used for the elaboration of the stimulation fluid were HCl (0.15 wt%) to dissolve carbonates, KCl (0.1 wt%) to stabilize clays, and acetic acid (0.01 wt%) to prevent metal precipitation. The formation and stimulation fluids have an Ionic Strength of 0.347 mol/Kg and 0.076 mol/Kg, respectively. The key to TD-NMR analysis is the relaxation response, represented by the transverse relaxation time T_2. Both fluids have a similar T_2 bulk response initially, with a value of 2350 ms for the formation fluid and 2440 ms for the stimulation fluid. We did not observe any changes in T_2 over time, which validated steps to avoid evaporation.

Table 1: Composition (mmol/kg) of Baxter Formation fluid and stimulation fluid. Modified from Edgin et al. [34], Edgin [35]

	pH	Eh (V)	Cl^-	$SO_4{}^{2-}$	SiO_2	Na^+	K^+	Ca^{2+}	Mg^{2+}	$HCO_3{}^-$	Fe*	Al^{3+}	C.B.E.(%)
Baxter Shale Formation Fluid	6.7	-0.24	325	.04	1.17	303	4.7	8.84	.309	2.62	.032	.0005	0.1
Stimulation Fluid	1.8	1.08	56.9	9.2	.37	22.8	13.8	4.28	6.96	24.4	0.0006	0	4.1

* Fe represent the total iron in solution including Fe^{2+} and Fe^{3+}

% C.B.E. is Charge Balance Error

3. Methods

3.1. Experimental approach

Two sets of reactive batch experiments were performed. The first set (Set A) was conducted at reservoir conditions (125 °C, 45 MPa) by Edgin et al. [34] and Edgin [35]. The main purpose of the first set of experiments was to analyze changes in the mineralogy and aqueous geochemistry, and thereby identify scenarios of mineral precipitation/dissolution and analyze changes in the pore architecture. The second set (Set B) of experiments at laboratory conditions (0.08 MPa, 25°C) was run with similar mass ratios to those in experiments at reservoir conditions; pressure is lower than standard pressure due to the effect

of elevation at our location. The purpose of the second set was to monitor rock matrix changes as reactions occurred, understand the role of the formation fluid and the OM without altering pore fluid saturation. While the information obtained from Set B could exhibit quantitative differences with data from Set A, the results gained us insights into the role of the two variables of interest. Moreover, this second set allowed us to study the effect of only the stimulation fluid on the rock matrix, when the pre-saturation step with formation fluid fluid was skipped. A summary of the experimental approach and the identification codes for each performed experiment are provided in the diagram in Figure 1. Each experiment described in the diagram has a unique identifier corresponding to set and assay number. In this order, 1A corresponds to the first experiment in Set A and 1B to the first experiment in Set B.

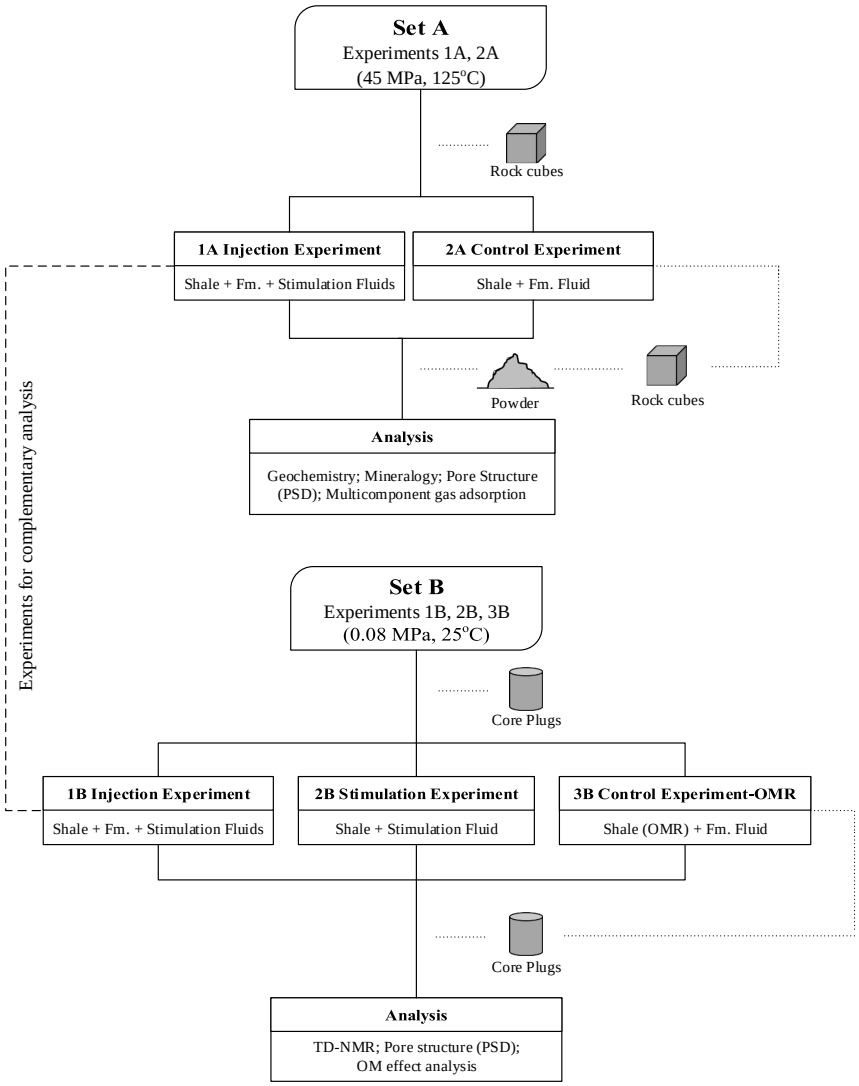

Figure 1: Diagram describing the experimental approach used in this study. In addition, a visual summary of sample treatment prior experiments and prior analysis is shown. (Fm.= Formation; OMR= Organic Matter Removed)

Rock properties from the first experimental set (Set A) were analyzed through gas adsorption before and after reactions. N_2 gas adsorption at 77K and CO_2 adsorption at 273K were used for the analysis of surface area and pore struc-

ture changes. CH_4 at 273K is used along with the CO_2 adsorption data to reveal changes in storage capacity and shed light on changes of surface properties related to wettability. The analysis of the second set (Set B) relied on Time Domain Nuclear Magnetic Resonance (TD-NMR). The same technique was also applied on glass-bead packing as a proxy for wettability alteration. N_2 isotherms were collected for samples from experiments 1B and 2B and jointly interpreted with NMR results to gain information on the role of the formation fluid. In addition, the role of the OM was investigated by comparing data from gas adsorption and TD-NMR characterization with and without OM. However, samples that underwent OM extraction were not used for any injection experiments, since the samples treatment could negatively impact the reactive process and introduce undesired changes. Additional details on the two set of reaction experiments are provided in sections 3.4 and 3.5.

3.2. Rock samples preparation

Shale used in the two experiments part of Set A at reservoir conditions (Experiments 1A and 2A, Figure 1) were cut to 0.5-1 cm^3 cubes prior to reaction. At the conclusion of these two experiments, reacted cubes were crushed and separated through a set of sieves: # 18 (1mm), # 40 (0.425 mm) and # 120 (0.125 mm). Samples bits between 0.425 and 1 mm in size were used on N_2, CH_4 and CO_2 adsorption experiments. The use of crushed samples aimed at avoiding problems related to gas diffusion into samples, to reduce the experimental times and to better focus on meso and micropores. Samples used for N_2 physisorption were vacuum-degassed for 24 hours at 110°C, prior to the experiment. Samples for CO_2 and CH_4 adsorption were additionally vacuum-degassed at 110°C for 12 hours. Effects of sample size, heterogeneities and reproducibility were evaluated from the same location in the core and compared to results of N_2 adsorption isotherms with those in Edgin et al. [34], Edgin [35]. We found that despite the possible artifacts in surface area and minor variability introduced from crushing, the result of the analysis did not show any significant discrepancy that could compromise the interpretation of results.

Shale core-plugs 1 cm in length and 0.8 cm in diameter were prepared to be used in experiments 1B, 2B and 3B (Figure 1). Shale samples underwent a vacuum-degassing process at 110°C prior to their use. A selected group of samples underwent a hydrogen peroxide extraction process to remove the organic matter, following the procedure used by Kuila et al. [51]. The group of samples corresponded to a crushed unreacted rock, crushed samples obtained from the control (2A) and injection (1A) experiments. In addition, an accelerated solvent extractor from Thermo Scientific was used to remove organics from one core-plug prior to its use in experiment 3B. The extraction was performed at 50°C and 10 MPa using Toluene as solvent. Extraction cycles were conducted until no change in solvent color was observed. Changes in organic content were analyzed through a Combustion Elemental Analyzer by determining the total organic carbon content. The carbon content was observed to decrease from around 2% to below 0.1%.

3.3. Glass beads preparation

To alter glass beads wettability with the 5% dimethyldichlorosilane in toluene solution, we followed Medina-Rodriguez et al.'s procedure [48]. Thereafter, the glass beads (OW and WW) were placed into the NMR-sample tubes maintaining a fluid-to-solid weight ratio of 0.5, warranting a height of 1 cm and avoiding the presence of free water. The free space in the samples tube was reduced by introducing a Teflon plug, which also allowed us to minimize the possible effects of evaporation. Details of the Time-Domain Nuclear Magnetic Resonance (TD-NMR) instrument are provided in the subsection on TD-NMR.

3.4. Set A experiments at reservoir conditions (1A, 2A)

The Injection Experiment (1A in Figure 1) reacted shale cubes and formation fluid for 1152 hours at 45 MPa and 125°C with an initial water/rock mass ratio of 20.7:1. Shale and formation fluid approached geochemical equilibrium and shale pores became saturated with formation fluid during this portion of the experiment. Stimulation fluid was subsequently injected into the ongoing

experiment resulting in a formation fluid/stimulation fluid/rock mass ratio of 13.6:5.8:1; the experiment continued an additional 640 hours. This approach contrasts with other experimental studies in which stimulation fluid and rock are combined at the outset of the experiment, before heating and pressurizing to reservoir conditions [17, 18, 29]. The Control Experiment (2A in Figure 1) reacted shale and formation fluid, but no stimulation fluid was added. The Control Experiment had an initial water/rock mass ratio of 18.6:1 and was conducted for 647 hours. The experimental procedure is described in detail in Edgin et al. [34], Edgin [35].

3.5. Set B experiments at laboratory conditions (1B, 2B, 3B)

The second set of experiments at laboratory conditions (Set B in Figure 1) was performed at similar fluid/solid ratios as Set A experiments. Samples for two replicas of the injection experiment (1B) were initially saturated with the synthetic formation fluid at 10 MPa (1450 psi). Subsequently, the rock-plugs were extracted from the saturation cell and placed in glass vials. Formation fluid was then added to the system until the desired ratios were attained. From this point on, the reactions were allowed to proceed at laboratory conditions (25°C and 0.08 MPa) for 30 days. After the aforementioned period elapsed, the stimulation fluid was added to the system until a similar water/stimulation fluid/rock ratio with respect to that of experiment 1A was achieved (13.6:5.8:1). The reaction was monitored for 60 days after the addition of the stimulation fluid.

Two replicas of experiment 2B were performed to analyze the shale-stimulation reaction without the pre-saturation step (reaction with formation fluid). Rock plugs were saturated at 10 MPa (1450 psi), and later placed in glass vials and additional stimulation fluid was added until a stimulation fluid/rock ratio of 19.4:1 was attained. Experiment 2B was intended to contrast with experiment 1B and shed light regarding the role of the synthetic formation fluid on the pore architecture alteration.

It is important to clarify that the reactions and rock matrix alteration that

take place in Set B samples are not completely equivalent to those taking place in Set A samples at reservoir conditions. Despite differences in equilibrium coefficients, rate constants of chemical reactions and the alteration introduced by the disruption of the reaction, the experiments should serve for analysis purposes. Due to the variability introduced by the experimental procedure, the aqueous phase was not analyzed in this set of experiments.

Finally, one core plug that underwent an organic extraction process was reacted with the formation fluid (experiment 3B). The saturation process was similar to that of experiments 2A and 2B. The final water/rock ratio was 20.7:1. Experiment 3B was performed with the purpose of understanding the role of the organic matter during the equilibration period of the rock and the formation fluid, and investigate its role in the possible rock changes.

3.6. Multicomponent Gas Adsorption

N_2 and CO_2 gas adsorption are used to examine the pore architecture. N_2 is used mainly for the analysis of mesopores and CO_2 for micropores. In addition, we conducted atypical CH_4 adsorption experiments, which corresponded to low-pressure/low-temperature conditions (0.08 MPa, 273 K), in contrast with traditional high-pressure/high-temperature conditions. N_2 along with CO_2 adsorption data have been widely used for shales pore structure characterization [36–39, 41, 42]. In contrast, CH_4 adsorption has been shown to relate more to changes in wettabilty, rather than structural ones [43]. Additionally, changes in wettability have been shown to affect adsorption significantly, and in some cases adsorption values have been halved by this effect [24]. The main original motivation for the use of low temperature/low pressure was due to the small size and amount of the samples. On the positive and novel side, this approach reduces the effects of any stress-induced changes and avoids the implication of the analysis of supercritical vapor. Low-pressure adsorption experiments have been previously used to assess intake capacities of porous media such as MOFs (Metal Organic Frameworks), where CO_2 and CH_4 adsorption data have been shown to be sensitive to surface properties of the porous material due to their

molecular characteristics and the difference in the related heat of adsorption [52, 53]. This is the first reported use of these low-temperature/low-pressure experiments for CH_4 in the context of shale characterization.

The data obtained from the adsorption experiments correspond to isotherms for different gasses. Whereas the CO_2 and CH_4 isotherms can be used directly to gain an insight about changes on rock surface properties (e.g. wettability), to obtain structural characteristics, inversion methods are needed. BET (Brunauer–Emmett–Teller) and BJH (Barrett-Joyner-Halenda) [54] theories are applied to the N_2 isotherm to obtain surface area and pore-size distribution, respectively. BET relies on a multilayer adsorption on a solid surface to determine the specific surface area of a material and BJH is related to the capillary condensation process taking place after the multiple layer adsorption have taken place, assuming a cylindrical pore shape. The pore-size distribution of micropores, on the other hand, was obtained from the CO_2 adsorption data through DFT (Density functional Theory) model [55, 56] assuming carbon-slit pores. DFT differs from BJH in that it is based on molecular dynamics instead of capillary condensation theory. This allows DFT to provide a better representation of the micropore structure. Inversion methods were applied using the Microactive software from Micromeritics.

Nitrogen physisorption isotherms were collected on powders derived for experiments 1A and 2A using an ASAP 2020 (Micromeritics) at 77 K (-196°C). CO_2 adsorption and methane adsorption/desorption data were collected on a HPVA II (Micromeritics) system in a pressure range from 0.01 to 0.08 MPa at 273 K (0°C). For the CO_2 adsorption data, 40 to 50 points were collected. CH_4 acquisition interval was divided into a 30-40 points range for the adsorption curve and a 25-30-point range for the desorption curve. The number of points was determined for each sample to reduce the noise-to-signal ratio. N_2 results in this work corresponded to a reanalysis of the samples from experiments 1a and 1b. Results were compared to those reported by Edgin et al. [34], Edgin [35] and no significant difference was found.

Additional N_2 adsorption experiments were performed on core samples from

the injection (1B) and stimulation (2B) experiments at the culmination of the reaction periods. Since core plugs were not crushed, the number of points for adsorption was reduced and the equilibration time was extended. The experimental setup at the time of these experiments did not allow the use core plugs for CO_2 and CH_4 analysis, so adsorption data were not collected.

3.7. Time Domain NMR

NMR relaxometry was selected due to its potential as a characterization technique [57] and sensitivity to changes in the rock properties. The most commonly used relationship to correlate pore structure to relaxation time follows[58]:

$$(1/T_2) = 1/T_{2\text{Bulk}} + \rho(S/V) \tag{1}$$

where T_2 is the transverse relaxation time from the experiment, $T_{2\text{Bulk}}$ is the relaxation time of the fluid used, ρ is the surface relaxivity and S/V is the surface-to-volume ratio of the pore space, which relates to the pore shape factor [59]. Although the technique has some constraints to quantitatively characterize small pores [60–64], it still represents a useful tool for a qualitative analysis of changes occurring in the rock such as saturation changes, pore structure and wettability alteration [31, 44–46].

TD-NMR (T_2) data were collected exclusively on samples from the second set of experiments (1B, 2B, 3B). Measurements were perfomed with an mq20 minispec (19.65 MHz) spectrometer from Bruker Biospin, attached to a F12-MA Julabo temperature control system, allowing the maintenance of temperature at 25±0.02°C into the probe. A standard Carr-Purcell-Meiboom-Grill (CPMG) pulse sequence was used to collect T_2 relaxation data [65]. Data for glass beads was obtained using 6500 echoes with a 90°-180°, pulse separation (τ) of 1 ms and a total of 64 scans. Meanwhile, a total of 3000 echoes were collected for the shale cores, using a τ of 0.05 ms and 400 scans. T_2 measurements for the replicas of experiment 2A were conducted right after the saturation process and after 15 and 30 days. Once the stimulation fluid was added to the system, T_2 data were collected after 30 and 60 days. The analysis of the experiment 3B

and the replicas of experiment 2B were performed after the saturation period and on days 15 and 30. Each relaxation experiment was run three times on each sample to account for variability on the relaxation time distribution. T_2 distribution data for all samples were obtained by decovolution using CONTIN software from Bruker Biospin.

4. Results from Set A experiments (1A, 1B)

4.1. Mineral dissolution and precipitation

Injection of stimulation fluid changed the aqueous geochemistry of the Injection Experiment in a manner consistent with dissolution of calcite and aluminosilicate minerals and precipitation of barite and clay [34, 35]. Mineral analysis using x-ray diffraction and scanning electron microscopy identified calcite dissolution textures and neoformed barite, but no evidence for aluminosilicate mineral dissolution or secondary clay mineralization was observed. The redox state of the Injection Experiment was controlled by equilibria between shale and formation fluid and not oxidized stimulation fluid. Dissolution of carbonate minerals is universally observed in experimental studies that react unconventional reservoir rock and acidic stimulation fluid [17, 18, 29], and barite scale is common in many of these experiments [29, 66–68]. Reaction of reservoir rock with acidic stimulation fluid dissolves feldspar and precipitates clay in several studies [29, 69] whereas no aluminosilicate reaction was observed in others [70]. Reaction of oxidizing stimulation fluid and shale controls the redox state in most experimental studies, leading to pyrite or pyrrhotite oxidation and formation of Fe(III)-(oxy) hydroxides [67, 70]. Mineral precipitation and dissolution are not the only possible changes that can occur in the rock. Surfaces properties (wettability) or the Organic Matter (OM) mass can also be altered [26, 28, 71, 72]. However, mass, structure and surface changes related to the OM can be addressed through the application of gas adsorption and TD-NMR analysis.

4.2. Structural analysis

The pore-size distributions for three samples are depicted in Figure 2. The first sample corresponded to a pristine rock identified as Unreacted ("square"). The second sample is the result of experiment 2A and was named Control ("circle"). The third sample comes from experiment 1A and is identified as Injection ("diamond"). Isotherms of all samples can be classified as Type II with an H4 hysteresis loop, characteristic of porous material with measurable volume of micropores [73, 74]. All samples exhibited a bimodal distribution from the BJH-PSD for the meso and macro-pores (>2 nm) as shown in Figure 2b, and similar behavior is obtained from the DFT Carbon-slit-PSD at the micro-porosity (Figure 2a). Data corresponding to the micropore analysis (PSD) are not shown in logarithmic scale for clarity purposes.

No appreciable effect induced by the reactions was observed on the PSD and the cumulative pore volume for the mesopore (Figure 2b and 2d) or the PSD for micropores (Figure 2a). The apparent limitation of the structural changes to the macropores was firstly reported by Edgin et al. [34], Edgin [35]. However, deeper understanding of changes in the system was needed, which served as motivation for the current study.

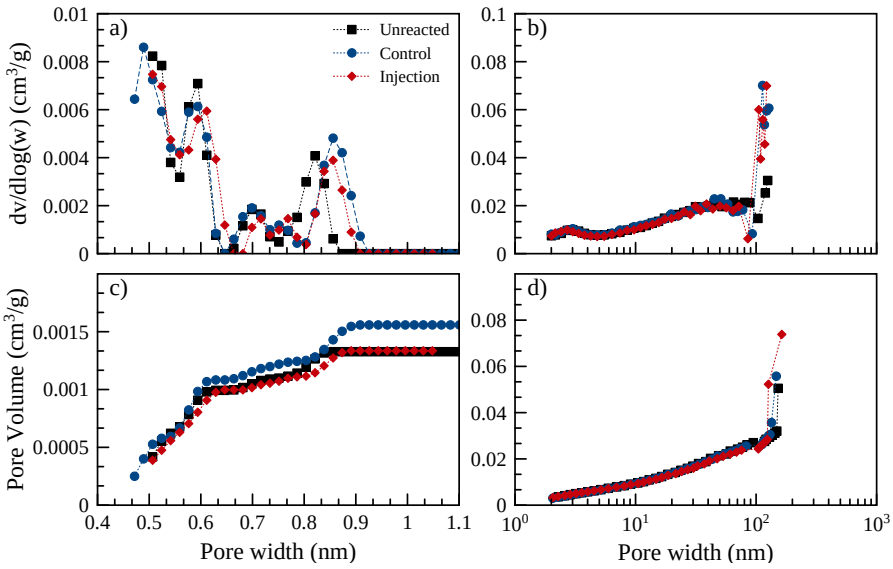

Figure 2: a) Pore-size distribution (Micropores) of the three samples obtained from DFT carbon-slit model applied to the adsorption of CO_2 at 273 K; b) Pore-size distribution (Meso-Macropores) of the three samples obtained from BJH model applied to the adsorption branch of the N_2 isotherm at 77 K*; c) Cumulative pore volume of the three samples obtained from the adsorption of CO_2 at 273 K; d) Cumulative pore volume of the three samples obtained from the N_2 adsorption at 77K*

*Samples from experiments A1 and A2, reprocessed and compared with results in Edgin et al. [34], Edgin [35]

The cumulative pore volume calculated from the CO_2 data (Figure 2c) shows a slight increase on the trend for the control sample (Control). This different response of the sample (Control) does not necessarily represent a change in the micro-pores. It is important to take into account that CO_2 intake capacity can be affected by changes of surface properties and interactions with the OM [75, 76]. In addition, the format chosen to show the results (linear scale) has a magnifying effect over the difference in the data. Surface area of the sample after contact with synthetic formation fluid, shows an increment(8.812 m^2/g to 10.067 m^2/g), which along with the behavior of the cumulative curve for the control sample ("circle") on Figure 2d, could be an indicative of rock surface alteration. However, additional information is needed. Other isotherm char-

acteristics such as the total pore volume and micropore volume remain similar among all samples.

All results show that processes of mineral dissolution and precipitation are minimal or null in micro- and mesopores. However, the use of physisorption analysis is limited at providing a complete description of the system; therefore, this needs to be complemented with other techniques that in the case of our work it corresponds to the application of TD-NMR.

4.3. CO_2 and CH_4 intake capacities

CO_2 adsorption isotherms were collected for the purpose of assessing the micropore structure. However, these isotherms can also be used to draw information on surface alteration. Molecular characteristics of CO_2 make these isotherms more sensitive to changes on the surface of the adsorbent. High-pressure CH_4 adsorption has been a common reference for storage capacity and has shown to be sensitive to changes in the pore architecture and surface properties. In this work, CH_4 isotherms were collected at low pressure and low temperature due to a reduced amount of sample available. However, the use of the selected conditions reduces the effect of any stress-induced changes and avoids the implication of the supercritical behavior of gases. The latter implies a better resolution for the purpose of surface and pore architecture analysis. CO_2 adsorption curves in Figure 3a exhibit a similar behavior, but the control sample ("circle") shows a deviation from the Injection ("diamond") and Unreacted ("square") samples. CH_4 isotherms (Figure 3b) exhibit hysteresis that is characteristic of materials with a wide pore-size distribution and with micropores [52, 74] and it shows a deviation from the other samples as well.

The difference in the amount of CO_2 and CH_4 adsorbed by the sample is not just related to pore accessibility, since both molecules have similar kinetic diameters (0.330 nm for CO2 and 0.380 nm for CH_4), but also to differences in polarity between CO_2 (possessing a quadrupole moment) and CH_4 (non polar) [53]. In other words, characteristics of the CO_2 molecule make it a more sensitive probe of changes in the sample.

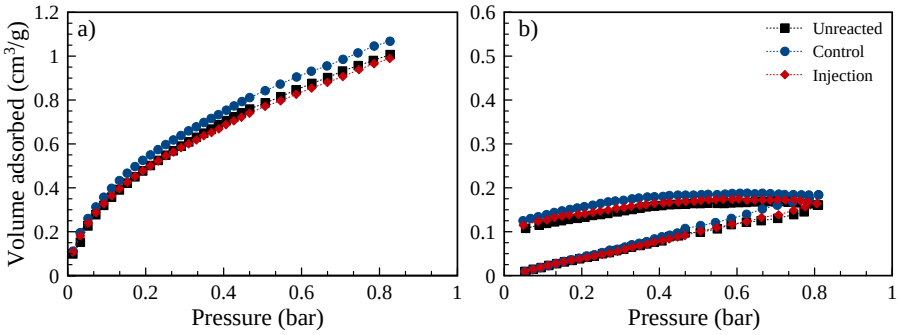

Figure 3: a) CO2 adsorption data of the three samples at 273 K b) Methane adsorption and desorption data for the three samples obtained a 273 K.

As mentioned in the previous section, the difference in the amount of CO_2 absorbed on the control samples ("circle") can result from a rock surface alteration during interaction with the synthetic formation fluid. To confirm the occurrence of surface alteration, the interpretation of the CH_4 isotherms must be added to the analysis. It has been shown that wettability may be more important than pore structure at determining the methane adsorption capacity [43]. Among the mechanisms driving wettability alteration, changes in salinity and water composition have been shown to be the most important factors influencing changes on this property [28].

Compiling the results from the PSD that show a minuscule change in the micro and mesopore region, (Figure 2a and 2b), the observed changes in surface area and the behavior of the CO_2 and CH_4 adsorptions (Figures 3) provide evidence of surface alteration, especially in the control experiment. However, experiment 1B and the TD-NMR analysis were performed to gather additional information regarding the alteration of the rock matrix during each injection experiment step.

5. Results Set B experiments at laboratory conditions (1B, 2B, 3B)

5.1. NMR response of glass beads

T_2 distribution data for glass beads was obtained to help guide the analysis of surface properties alteration (wettability) in rock samples, following the procedure described in Medina-Rodriguez et al. [48]. Figures 4a and 4b correspond to the T_2 distribution of Oil-Wet (OW) glass beads with formation fluid and stimulation fluid, respectively. Figures 4c and 4d show the response of Water-Wet (WW) glass beads. The T_2 distributions show that the formation fluid and the stimulation fluid can induce surface (wettability) alteration, a phenomenon identified by the shift on the main peak locations of the T_2 distribution for the OW glass beads samples (Figure 4a and 4b). Formation fluid induces a displacement from 1556 ms to 1338 ms and the stimulation fluid produces a peak displacement from 1879 ms to 1743 ms.

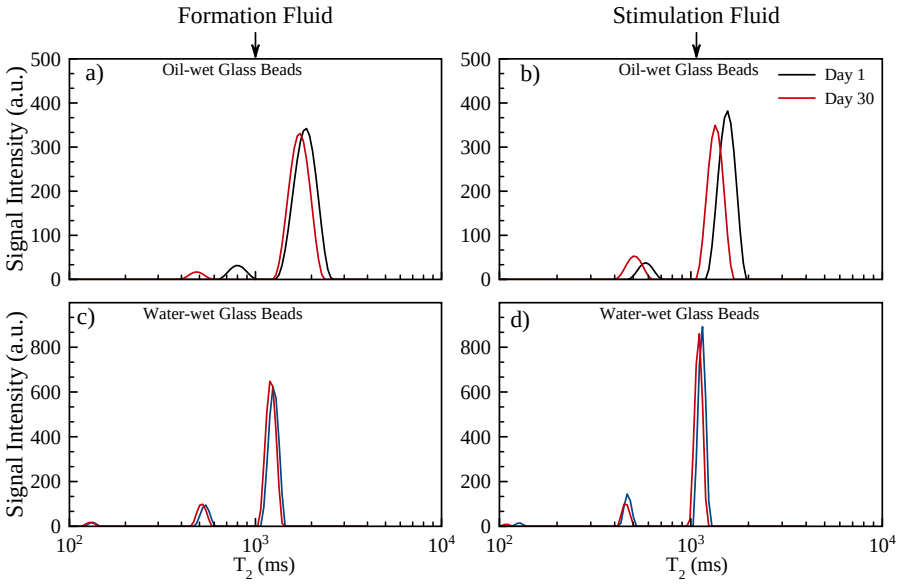

Figure 4: a) T_2 distribution of Altered (OW) glass bead saturated imbibed in formation fluid for 30 days b) T_2 distribution of Altered (OW) glass bead saturated imbibed in stimulation fluid for 30 days c) T_2 distribution normal (WW) glass bead saturated imbibed in formation fluid for 30 days d) T_2 distribution of normal (WW) glass bead saturated imbibed in stimulation fluid for 30 days.

The stimulation fluid appears to be more effective at inducing a surface alteration (Figure 4b). The larger peak displacement can be the result of the low salinity and/or the lower pH of the fluid. This behavior has been observed on systems similar to shales [45]. However, further analysis at the nanometer scale is required, but it is out of the scope of this study.

5.2. NMR response of the injection experiment (Experiment 1B)

Figure 5 shows the T_2 distribution of the plug samples from the two replicas of experiment 1B, sample 1 (Figure 5a) and sample 2 (Figure 5b). The curves correspond to the interaction of the rock with formation fluid on days 1 and 30. The trend followed by the two samples are similar, demonstrating the reproducibility of the method and showing the alteration mechanisms are dominant, despite possible differences between samples.

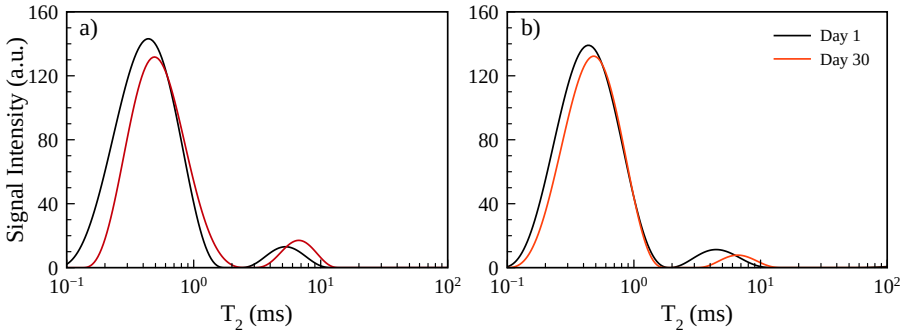

Figure 5: a) T_2 distribution of Baxter shale saturated and reacted with formation fluid for 30 days (sample 1) b) T_2 distribution of Baxter shale saturated and reacted with formation fluid for 30 days (sample 2)

The T_2 distribution shows a general shift for both samples, while the general shape remains similar. The displacement of the dominant peak has been observed in wettability analysis of other systems, i.e. coal and sandstone [45, 48], and the shift has been shown to relate to differences on the surface relaxvity of the porous media, which in turn is linked to surface properties (wettability). The evidence from glass bead experiments shows that formation fluid can induce surface alteration (Figure 3a) and results at this stage of experiment 1B

suggest that surface alteration would be the dominant mechanism affecting the rock while in contact with the formation fluid.

Figure 6 shows the T_2 distribution of samples 1 and 2 (Figures 6a and 6b) after the addition of the stimulation fluid. The distribution labeled "Day 30" corresponds to the last measurement conducted prior to the addition of the stimulation fluid. The data presented as "Day 60" and "Day 90" correspond to 30 and 60 days of reaction time after the addition of the stimulation fluid.

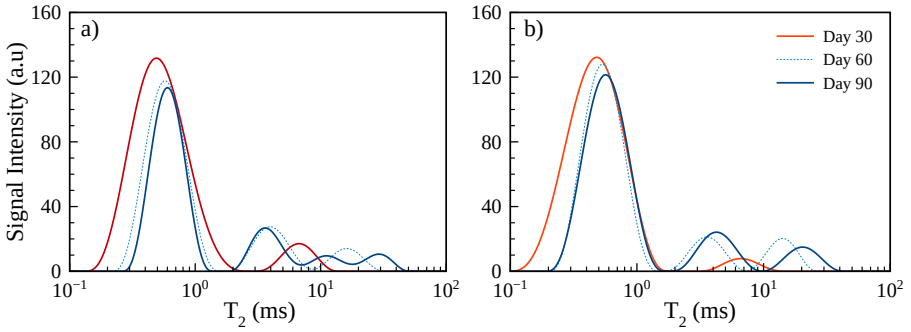

Figure 6: a) T_2 distribution of Baxter shale (sample 1) initially saturated with formation fluid and reacted with stimulation fluid for 60 days; b) T_2 distribution of Baxter shale (sample 2) initially saturated with formation fluid and reacted with stimulation fluid for 60 days

Data for days 60 and 90 show a significant change in the T_2 distribution, especially for longer relaxation times (>5 ms). New peaks emerged, suggesting a clear structural change in the shale plug, possibly related to microfractures formation or propagation as well as to mineral precipitation and dissolution [20, 44, 46, 77]. Minor changes in the T_2 distribution for times close to 1 ms may indicate that the smaller pores have not been significantly altered or can be the effect of the fluid distribution within the pores.

NMR analysis of experiment 1B is consistent with the observations from the gas adsorption from Set A experiments at reservoir conditions. For example, changes in the T_2 distribution at the end experiment 1B (Figure 6) can be contrasted with the PSD presented in Figures 2a and 2b. Both results suggest that the injection process (addition of stimulation fluid), if samples are presaturated

with formation fluid, leads to a change in the pore structure that is more significant in the macropore region. On the other hand, the interaction with the formation fluid during experiment 1B (Figure 5) can be analyzed using CO_2 and CH_4 adsorption results from Set A experiment (Figure 3) that correspond to the same system under different reactive conditions. In this case, both results show surface alteration as the dominant mechanism controlling the changes in the rock matrix while rock interacts with the formation fluid.

5.3. Results from the stimulation experiment (2B)

Baxter Shale samples were reacted directly with the stimulation fluid (experiment 2B), in order to gather additional information on the role that the formation fluid plays during the stimulation process. Changes in the T_2 distribution (Figure 7a) and those of the PSD (Figure 7b) show that the stimulation fluid, without the presaturation step, can affect the pore architecture at all scales. This important observation warns on the risk of interpreting reactive experiment results without incorporating native fluids as the initial condition.

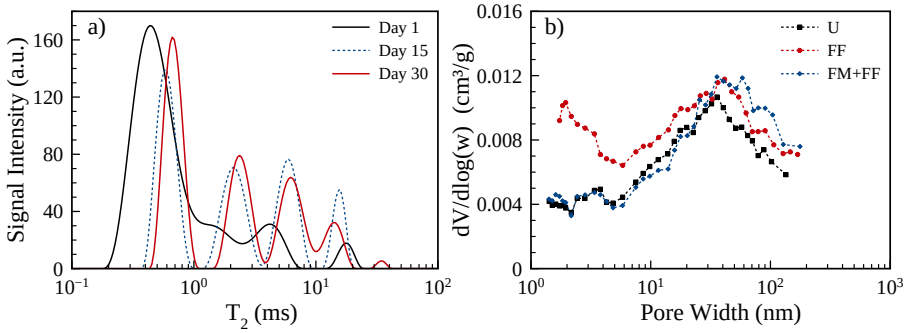

Figure 7: a) T_2 distribution of Baxter shale saturated and reacted with stimulation for 30 days; b) PSD of unreacted Baxter (U), Baxter shale from injection experiment-2A (FM+FF) and Baxter reacted with stimulation fluid experiment-2C(FF)

Figure 7a shows that the stimulation fluid can induce a significant change in the rock, even after only 15 days of reaction time. Contrasted with the results considering formation fluid of experiment 1B (Figure 5), it is possible to say that the stimulation fluid induces changes even right after the saturation period.

Figure 7b shows the PSD of an unreacted core-plug (U - "square"), the sample directly reacted with stimulation fluid of experiment 2B (FF - "circle") and the sample that underwent experiment 2A (FM+FF - "diamond"). PSD results show that without the presaturation step, the stimulation fluid can reach and induce changes in the pore-architecture at all scales. In addition, results provide additional information to demonstrate that when formation fluid is present, changes in the pore structure are more significant in the macropore region.

6. Analysis upon organic matter removal

Results presented in the previous sections suggest that processes able to induce surface and pore structure alteration take place in the rock. These changes can be related to the OM, considering that OM has been shown to be a primary component in the wettability analysis. Therefore, additional evidence on the role of the OM in the reaction is needed.

6.1. Analysis of the Baxter Shale before and after organic matter removal

Results after removing the OM from an unreacted sample show a general increment of the pore volume along the entire pore-size distribution. The increment is evidenced on the PSD of the micro- and meso-pores data (Figure 8 a and b), as well as on the cumulative pore volume (Figure 8c and 8d).

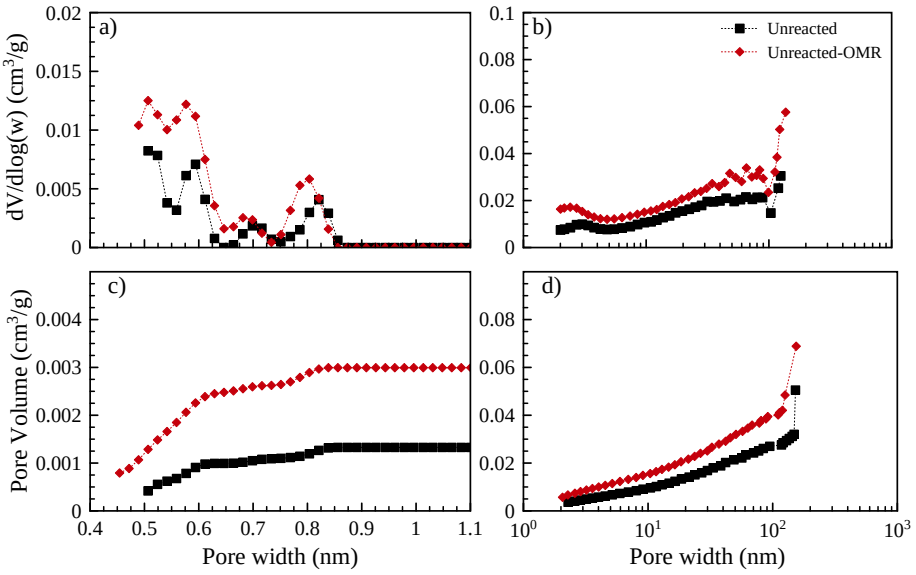

Figure 8: a) Pore-size distribution (Micropores) of Unreacted sample, before and after OM removal, obtained from DFT carbon-slit model applied to the adsorption of CO_2 at 273 K; b) Pore-size distribution (Meso-Macropores) of Unreacted sample, before and after OM removal, obtained from BJH model applied to the adsorption branch of the N_2 isotherm at 77 K; c) Cumulative pore volume of Unreacted sample, before and after OM removal, obtained from the adsorption of CO_2 at 273 K; d) Cumulative pore volume of Unreacted sample, before and after OM removal, obtained from the N_2 adsorption at 77K.

These increments could be explained by the fact that organic matter may be located in some pores in clay material, acting as a pre-filler of some nanostructures. Therefore, its removal translates into the exposure of some nano-pores that could not be hosted in the clays [51]. The blockage of pores due to the presence of OM was also observed by Saidian et al. [78] and was reported as one possible source of interference on adsorption data interpretation. CO_2 and CH_4 adsorption data, shown in Figures 9a and 9b, respectively, exhibit a considerable increment. This effect could relate to the exposure of the new porosity as well as to the increment of the available surface area after the organic matter removal. The latter is true, despite the fact that the amount of adsorption of these gases has always been closely related to the organic matter. The data

suggest that when the organic matter acts as a pore-blocking agent, it can as well negatively impact the storage capacity of the rock.

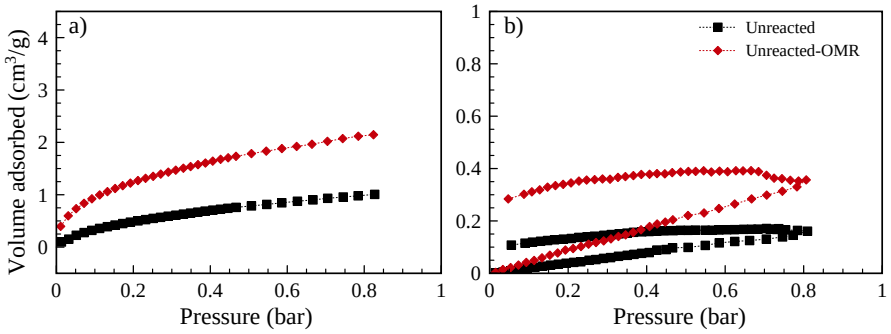

Figure 9: a) CO_2 adsorption data of Unreacted sample, before and after OM removal, at 273 K; b)CH_4 adsorption and desorption data of Unreacted sample, before and after OM removal, obtained at 273 K

The results obtained on the unreacted Baxter Shale, before and after the removal of OM, do not allow a quantitative determination of its mass. Used qualitatively, however, it could help to understand possible effects of the reaction procedure on the OM and to identify the role it plays. Data suggest that in the case of the Baxter Shale, the OM acts mainly as a gas-blocking agent, a concept that can be extended to the interaction with synthetic formation fluid and the stimulation fluid, which can be translated into the poor ability of the fluid to reach small pores.

6.2. Analysis of samples from experiments 1A and 2A after OM removal

After the OM was removed from the unreacted, control and injection samples, changes in isotherms were consistent for the three samples, corresponding to the behavior of an H3 hysteresis loop [34, 35]. Such behavior has been widely reported for shale rocks in which a considerable amount of micro-porosity exists [74]. Figure 10 shows the pore-size distribution and the cumulative pore volume from N_2 adsorption data. The changes with respect to the sample prior to organic matter removal (Figure 10) are consistent for the three samples, and again the data suggest pore structure alteration in the macro-pore region.

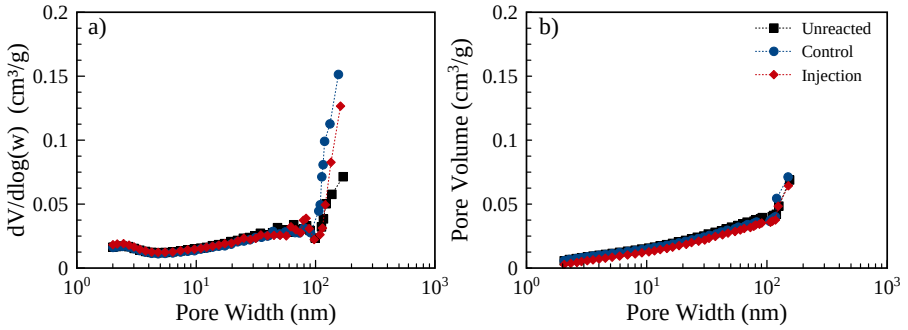

Figure 10: a) Pore-size distribution (Meso-Macropores) of the three samples, after OM removal, obtained from BJH model applied to the adsorption branch of the N_2 isotherm at 77 K; b) Cumulative pore volume of the three samples, after OM removal, obtained from the N_2 adsorption at 77K

These consistent changes along with the similar trends observed on the surface area, total pore volume and micro-pore volume with an average and similar difference of 14 (m^2/g), 0.03 (m_3/g) and 0.001 (cm_3/g), respectively, suggest that the amount of organic matter is not significantly altered during reactions.

6.3. NMR response of shale without OM and formation fluid (3B)

Organic matter was removed from one Baxter Shale plug. The plug was used to analyze the relaxation time response of a shale samples with a reduced amount of OM in contact with formation fluid for 30 days under standard conditions. The evolution of the T_2 distribution that result from this reaction is shown in Figure 11.

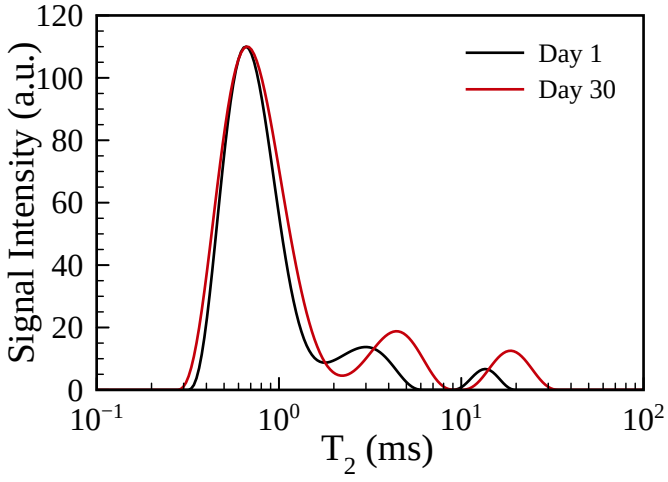

Figure 11: T_2 distribution of Baxter shale with reduced OM saturated with formation fluid and reacted for 30 day

Similar to Figure 5, which corresponds to the interaction of an untreated shale core with formation fluid, the general shape of the T_2 distribution remains similar and an apparent peak displacement takes place. This trend shows that despite the removal of OM, the shale sample undergoes a similar process. The latter suggests that the surface alteration is related, but not limited, to the presence of OM. It is important to mention that the treatment of the sample, i.e. removal of OM, can create artifacts in the analysis (e.g. the additional peak around 10 ms). In addition, it is not possible to determine if the totality of the OM was extracted and if the fluid used for OM removal can be totally removed from the sample. These two possibilities suggest that further analysis of these samples at laboratory or reservoir conditions would be biased. Therefore, stimulation fluid was not added to this system.

7. Discussion

The shale alteration is a compounded process of surface properties (wettability) and pore structure alterations. Such changes could occur throughout different pore sizes, from micropores to fractures. Surface property alteration,

commonly referred to as wettability alteration, seems to be more significant during the first contact of the rock with an exogenous fluid, as is implicit in most of experimental techniques used to address this question [21, 26, 27, 30, 31]. However, surface alteration is not limited to hydrophobicity or hydrophilicity; instead, it is a more complex process, involving changes in surface area, clay sites, ionic exchange and adsorption processes. On the other hand, structural changes have been shown to be a result of mineral dissolution and precipitation as well as the result of changes on the organic component of the system [16, 17, 29]. The complementary analysis of physisorption and TD-NMR data presented in this work proved to be an adequate approach for assessing the mechanisms that control the changes induced by rock-formation fluid-stimulation fluid interactions, in a diffusion-driven process, at different scale of the pore architecture. The difference in the adsorption of CO_2 and CH_4 (Figure 3) along with the change in surface area of the control samples from experiment 2A, and the general shift of the T_2 distribution during the first stage of experiment 1B (Figure 5), suggest that surface properties alteration and a minor mineral dissolution are the dominant phenomena controlling changes induced by the equilibration process between the rock and the formation fluid. The surface alteration could be associated with minor differences between the synthetic and the real formation fluid, until the system is at equilibrium. In the literature, wettability alteration has been reported to have a relationship with differences in salinity of fluids [28]. The minor mineral dissolution can be limited to rock surface that is in direct contact with the fluid and can be related to changes in the macropores (Figure 2b). The subsequent process, corresponding to reaction with the stimulation fluid, seems to be mainly influenced by pore structure alteration. This can be corroborated by the changes in the T_2 distribution at longer relaxation times (> 3 ms) from experiment 1B (Figure 6), along with the changes on the macroporosity observed in the physisorption experiment of the Injection samples from experiment 1A (Figure 2). Such pore structure changes result in changes in the transport properties and the gas intake capacity of the rock. This process is mainly governed by mineral dissolution and precipitation, while the role of

wettability alteration is significantly diminished. In addition, data suggest that the diffusion-driven alteration among the three-component systems will not significantly affect pores located in the meso and micro-pore region, since fluid displacement is limited. The rock matrix alteration may not be immediately reflected on the overall transport properties such as permeability. However, this alteration may affect transport in the long term. Results also shed light on why reported results differ from one another, despite the similarities in the material or components used to carry out the reaction. The addition of the formation fluid as an intermediate state of the reaction analysis could connect better with real reservoir systems, where formation fluid is always present. In spite of the fact that the formation fluid can be displaced by the injection fluid, the total initial saturation would not be removed and not all pores would be accessible. Results for the unreacted rock before and after OM removal, show that OM represents an accessibility restriction to some nano-pores, further implying a restriction for the fluid of interest to access those pores and suggesting that the possible changes are related to the distribution of the OM in the rock. Differences in the pore-size distribution of the unreacted and those from experiments 1A and 2A, before (figures 2b and d) and after (Figures 10a and b) organic matter removal, suggest the organic matter is not being significantly altered. Finally, results from experiment 3B show that, despite the absence of OM, the equilibration process with the formation fluid can still induce surface alteration. Further investigation of this process is needed. In this work, we provide evidence on the role that the formation fluid and OM play in the interaction with a stimulation fluid at different scales of the pore architecture. However, more work is needed.

8. Conclusions

1. Structural changes dominate over surface alteration during the reaction with the stimulation fluid, if the rock is presaturated with the formation fluid. The pore architecture alteration is more significant in the macropore

region

2. The equilibration process with the formation fluid induces surface alteration and mineral dissolution on the rock and its presence diminishes the effect of the stimulation fluid.
3. The organic matter role during reactions appears to be linked to its distribution in the rock. In the case of the Baxter Shale, the OM is a blocking agent that creates pore accessibility restrictions and have a minimal influence on mechanisms that control changes in the rock matrix.
4. TD-NMR and gas adsorption analysis complement each other in a way that allows a better understanding of changes induced by the stimulation process on the pore architecture and surface properties of the rock. TD-NMR offers the advantage of probing a broad pore size scale, which enables the analysis in presence of the saturation fluids. Gas adsorption of N_2 and CO_2 provides an adequate representation of the pore structure and the analysis of CH_4 and CO_2 provides evidence on surface alteration process.
5. Changes in rock properties are linked to the experimental procedure used to emulate the stimulation process. The pre-saturation step with a formation fluid provides a better representation of the reservoir conditions and consequently a better predictor of rock alteration.

Acknowledgment

This work was supported as part of the Center for Mechanistic Control of Water-Hydrocarbon-Rock Interactions in Unconventional and Tight Oil Formations (CMC-UF), an Energy Frontier Research Center funded by the U.S. Department of Energy, Office of Science under DOE (BES) Award DE-SC0019165.

Kaszuba's work was supported as part of the EFRC-MUSE, an Energy Frontier Research Center funded by the U.S. Department of Energy, Office of Science, Basic Energy Sciences under Award #DE-SC0019285.

References

[1] M. Binnion, How the technical differences between shale gas and conventional gas projects lead to a new business model being required to be successful, Marine and Petroleum Geology 31 (2012) 3–7.

[2] R. J. Davies, S. Almond, R. S. Ward, R. B. Jackson, C. Adams, F. Worrall, L. G. Herringshaw, J. G. Gluyas, M. A. Whitehead, Oil and gas wells and their integrity: Implications for shale and unconventional resource exploitation, Marine and Petroleum Geology 56 (2014) 239–254.

[3] Z. Wang, A. Krupnick, A retrospective review of shale gas development in the United States: What led to the boom?, Economics of Energy & Environmental Policy 4 (2015) 5–18.

[4] A. Abramova, V. Abramov, S. Kuleshov, E. Timashev, Analysis of the modern methods for enhanced oil recovery, Energy Science and Technology 3 (2015) 118–148.

[5] H. E. King Jr, A. P. Eberle, C. C. Walters, C. E. Kliewer, D. Ertas, C. Huynh, Pore architecture and connectivity in gas shale, Energy & Fuels 29 (2015) 1375–1390.

[6] C. Liu, H. Liu, Y. Zhang, D. Deng, H. Wu, Optimal spacing of staged fracturing in horizontal shale-gas well, Journal of Petroleum Science and Engineering 132 (2015) 86–93.

[7] X. Cao, M. Wang, J. Kang, S. Wang, Y. Liang, Fracturing technologies of deep shale gas horizontal wells in the Weirong Block, Southern Sichuan Basin, Natural Gas Industry B 7 (2020) 64–70.

[8] H. Zhang, J. Sheng, Optimization of horizontal well fracturing in shale gas reservoir based on stimulated reservoir volume, Journal of Petroleum Science and Engineering 190 (2020) 107059.

[9] R. Barati, J.-T. Liang, A review of fracturing fluid systems used for hydraulic fracturing of oil and gas wells, Journal of Applied Polymer Science 131 (2014).

[10] Z. Sun, Y. Ni, Y. Wang, Z. Wei, B. Wu, J. Li, W. Fan, G. Wang, Y. Li, Experimental investigation of the effects of different types of fracturing fluids on the pore structure characteristics of shale reservoir rocks, Energy Exploration & Exploitation 38 (2020) 682–702.

[11] K. Makhanov, A. Habibi, H. Dehghanpour, E. Kuru, Liquid uptake of gas shales: A workflow to estimate water loss during shut-in periods after fracturing operations, Journal of Unconventional Oil and Gas Resources 7 (2014) 22–32.

[12] R. A. Gonzalez, X. Gong, D. A. McVay, et al., Probabilistic decline curve analysis reliably quantifies uncertainty in shale gas reserves regardless of stage of depletion, in: SPE Eastern Regional Meeting, Society of Petroleum Engineers, 2012.

[13] H. Wachtmeister, L. Lund, K. Aleklett, M. Höök, Production decline curves of tight oil wells in Eagle Ford shale, Natural Resources Research 26 (2017) 365–377.

[14] B. Turley, M. A. Caretta, Household water security: An analysis of water affect in the context of hydraulic fracturing in West Virginia, Appalachia, Water 12 (2020) 147.

[15] R. D. Vidic, S. L. Brantley, J. M. Vandenbossche, D. Yoxtheimer, J. D. Abad, Impact of shale gas development on regional water quality, Science 340 (2013).

[16] M. K. Dustin, J. R. Bargar, A. D. Jew, A. L. Harrison, C. Joe-Wong, D. L. Thomas, G. E. Brown Jr, K. Maher, Shale kerogen: hydraulic fracturing fluid interactions and contaminant release, Energy & Fuels 32 (2018) 8966–8977.

[17] A. L. Harrison, A. D. Jew, M. K. Dustin, D. L. Thomas, C. M. Joe-Wong, J. R. Bargar, N. Johnson, G. E. Brown Jr, K. Maher, Element release and reaction-induced porosity alteration during shale-hydraulic fracturing fluid interactions, Applied Geochemistry 82 (2017) 47–62.

[18] A. D. Jew, M. K. Dustin, A. L. Harrison, C. M. Joe-Wong, D. L. Thomas, K. Maher, G. E. Brown Jr, J. R. Bargar, Impact of organics and carbonates on the oxidation and precipitation of iron during hydraulic fracturing of shale, Energy & Fuels 31 (2017) 3643–3658.

[19] Y. Kreisserman, S. Emmanuel, Release of particulate iron sulfide during shale-fluid interaction, Environmental Science & Technology 52 (2018) 638–643.

[20] D. Renock, J. D. Landis, M. Sharma, Reductive weathering of black shale and release of barium during hydraulic fracturing, Applied geochemistry 65 (2016) 73–86.

[21] H. Dehghanpour, H. Zubair, A. Chhabra, A. Ullah, Liquid intake of organic shales, Energy & Fuels 26 (2012) 5750–5758.

[22] E. Ghanbari, H. Dehghanpour, Impact of rock fabric on water imbibition and salt diffusion in gas shales, International Journal of Coal Geology 138 (2015) 55–67.

[23] P. Fakcharoenphol, B. Kurtoglu, H. Kazemi, S. Charoenwongsa, Y.-S. Wu, et al., The effect of osmotic pressure on improve oil recovery from fractured shale formations, in: SPE unconventional resources conference, Society of Petroleum Engineers, 2014.

[24] H. Abdulelah, S. M. Mahmood, A. Al-Mutarreb, Effect of anionic surfactant on wettability of shale and its implication on gas adsorption/desorption behavior, Energy & Fuels 32 (2018) 1423–1432.

[25] A. Neog, D. S. Schechter, et al., Investigation of surfactant induced wettability alteration in Wolfcamp shale for hydraulic fracturing and eor appli-

cations, in: SPE Improved Oil Recovery Conference, Society of Petroleum Engineers, 2016.

[26] H. Roshan, A. Al-Yaseri, M. Sarmadivaleh, S. Iglauer, On wettability of shale rocks, Journal of Colloid and Interface Science 475 (2016) 104–111.

[27] J. J. Sheng, Discussion of shale rock wettability and the methods to determine it, Asia-Pacific Journal of Chemical Engineering 13 (2018) e2263.

[28] L. Zeng, Y. Chen, M. M. Hossain, A. Saeedi, Q. Xie, Wettability alteration induced water uptake in shale oil reservoirs: A geochemical interpretation for oil-brine-om interaction during hydraulic fracturing, International Journal of Coal Geology 213 (2019) 103277.

[29] issolution of minerals and precipitation of an aluminosilicate phase during experimentally simulated hydraulic fracturing of a mudstone and a tight sandstone in the powder river basin, wy (????).

[30] Q. Xie, Y. Chen, L. You, M. M. Hossain, A. Saeedi, Drivers of wettability alteration for oil/brine/kaolinite system: implications for hydraulic fracturing fluids uptake in shale rocks, Energies 11 (2018) 1666.

[31] M. Josh, L. Esteban, C. Delle Piane, J. Sarout, D. Dewhurst, M. Clennell, Laboratory characterisation of shale properties, Journal of Petroleum Science and Engineering 88 (2012) 107–124.

[32] Z. Yushi, Z. Shicheng, Z. Tong, Z. Xiang, G. Tiankui, Experimental investigation into hydraulic fracture network propagation in gas shales using ct scanning technology, Rock Mechanics and Rock Engineering 49 (2016) 33–45.

[33] G. Cheng, B. Deng, Y. Liu, J. Chen, K. Wang, D. Zhang, M. Li, Experimental investigation on the feasibility and efficiency of shear-fracturing stimulation for enhancing coal seam permeability, Journal of Natural Gas Science and Engineering (2020) 103381.

[34] M. G. Edgin, B. Medina-Rodriguez, J. P. Kaszuba, J. C. Dewey, V. Alvarado, Gas shale pore-architecture alteration from geochemical reactions with stimulation fluid, Fuel , *submitted* (2021).

[35] M. G. E. Edgin, Subsurface Reactions in a Gas Shale: Effects of Stimulation Fluids on Porosity and Permeability in the Presence of Formation Water, Master's thesis, University of Wyoming, 2019.

[36] S. Bernard, B. Horsfield, H.-M. Schulz, R. Wirth, A. Schreiber, N. Sherwood, Geochemical evolution of organic-rich shales with increasing maturity: A stxm and tem study of the Posidonia Shale (Lower Toarcian, Northern Germany), Marine and Petroleum Geology 31 (2012) 70–89.

[37] G. R. Chalmers, R. M. Bustin, I. M. Power, Characterization of gas shale pore systems by porosimetry, pycnometry, surface area, and field emission scanning electron microscopy/transmission electron microscopy image analyses: Examples from the Barnett, Woodford, Haynesville, Marcellus, and Doig units: Characterization of Gas Shale Pore Systems, AAPG bulletin 96 (2012) 1099–1119.

[38] J. Chen, X. Xiao, Evolution of nanoporosity in organic-rich shales during thermal maturation, Fuel 129 (2014) 173–181.

[39] C. R. Clarkson, M. Freeman, L. He, M. Agamalian, Y. Melnichenko, M. Mastalerz, R. M. Bustin, A. Radliński, T. Blach, Characterization of tight gas reservoir pore structure using USANS/SANS and gas adsorption analysis, Fuel 95 (2012) 371–385.

[40] C. R. Clarkson, N. Solano, R. M. Bustin, A. Bustin, G. Chalmers, L. He, Y. B. Melnichenko, A. Radliński, T. P. Blach, Pore structure characterization of north american shale gas reservoirs using USANS/SANS, gas adsorption, and mercury intrusion, Fuel 103 (2013) 606–616.

[41] M. Mastalerz, L. He, Y. B. Melnichenko, J. A. Rupp, Porosity of coal and

shale: Insights from gas adsorption and SANS/USANS techniques, Energy & Fuels 26 (2012) 5109–5120.

[42] M. Schmitt, C. P. Fernandes, J. A. da Cunha Neto, F. G. Wolf, V. S. dos Santos, Characterization of pore systems in seal rocks using nitrogen gas adsorption combined with mercury injection capillary pressure techniques, Marine and Petroleum Geology 39 (2013) 138–149.

[43] P. Luo, N. Zhong, I. Khan, X. Wang, H. Wang, Q. Luo, Z. Guo, Effects of pore structure and wettability on methane adsorption capacity of mud rock: Insights from mixture of organic matter and clay minerals, Fuel 251 (2019) 551–561.

[44] A. M. Gomaa, B. Zhang, Q. Qu, S. Nelson, J. Chen, et al., Using NMR technology to study the flow of fracture fluid inside shale formation, in: SPE International Symposium and Exhibition on Formation Damage Control, Society of Petroleum Engineers, 2014.

[45] X. Sun, Y. Yao, D. Liu, Y. Zhou, Investigations of CO_2-water wettability of coal: NMR relaxation method, International Journal of Coal Geology 188 (2018) 38–50.

[46] D. Veselinovic*, D. Green, M. Dick, Determination of natural fracture porosity using NMR, in: Unconventional Resources Technology Conference, San Antonio, Texas, 1-3 August 2016, Society of Exploration Geophysicists, American Association of Petroleum . . . , 2016, pp. 1062–1069.

[47] M. Longman, K. Dahlberg, K. Yared, et al., Lithologies and petrophysical characteristics of the upper cretaceous baxter shale gas reservoir, canyon creek field, sweetwater county, wyoming, in: SPE Low Perm Symposium, Society of Petroleum Engineers, 2016.

[48] B. X. Medina-Rodriguez, T. Reilly, H. Wang, E. R. Smith, G. Garcia-Olvera, V. Alvarado, S. Aryana, Time-domain nuclear magnetic resonance

determination of wettability alteration: Analysis for low-salinity water, Applied Sciences 10 (2020) 1017.

[49] E. Bolke, Dissolved-oxygen depletion and other effects of storing water in Flaming Gorge Reservoir, Wyoming and Utah, volume 2058, Department of the Interior, Geological Survey, 1979.

[50] I. O. . G. C. C. F. Groundwater Protection Council, Chemical Disclosure Registry, Entry 131205 ks, ???? URL: http://fracfocus.org/.

[51] U. Kuila, D. K. McCarty, A. Derkowski, T. B. Fischer, T. Topór, M. Prasad, Nano-scale texture and porosity of organic matter and clay minerals in organic-rich mudrocks, Fuel 135 (2014) 359–373.

[52] H. Furukawa, O. M. Yaghi, Storage of hydrogen, methane, and carbon dioxide in highly porous covalent organic frameworks for clean energy applications, Journal of the American Chemical Society 131 (2009) 8875–8883.

[53] J. Zhang, L. Sun, F. Xu, F. Li, H.-Y. Zhou, F.-L. Huang, Z. Gabelica, C. Schick, Hydrogen storage and selective carbon dioxide capture in a new chromium (iii)-based infinite coordination polymer, RSC advances 2 (2012) 2939–2945.

[54] E. P. Barrett, L. G. Joyner, P. P. Halenda, The determination of pore volume and area distributions in porous substances. i. computations from nitrogen isotherms, Journal of the American Chemical society 73 (1951) 373–380.

[55] R. Evans, P. Tarazona, Theory of condensation in narrow capillaries, Physical Review Letters 52 (1984) 557.

[56] P. Tarazona, Free-energy density functional for hard spheres, Physical Review A 31 (1985) 2672.

[57] Y.-Q. Song, R. Kausik, NMR application in unconventional shale reservoirs–A new porous media research frontier, Progress in nuclear magnetic resonance spectroscopy 112 (2019) 17–33.

[58] G. R. Coates, L. Xiao, M. G. Prammer, et al., NMR logging: principles and applications, volume 234, Haliburton Energy Services Houston, 1999.

[59] Y. Liu, Y. Yao, D. Liu, S. Zheng, G. Sun, Y. Chang, Shale pore size classification: An NMR fluid typing method, Marine and Petroleum Geology 96 (2018) 591–601.

[60] M. Fleury, E. Kohler, F. Norrant, S. Gautier, J. M'Hamdi, L. Barré, Characterization and quantification of water in smectites with low-field NMR, The Journal of Physical Chemistry C 117 (2013) 4551–4560.

[61] M. Fleury, M. Romero-Sarmiento, Characterization of shales using t1–t2 NMR maps, Journal of Petroleum Science and Engineering 137 (2016) 55–62.

[62] M. Fleury, J. Soualem, Quantitative analysis of diffusional pore coupling from T_2-store-T_2 NMR experiments, Journal of Colloid and Interface Science 336 (2009) 250–259.

[63] M. Mehana, I. El-monier, Shale characteristics impact on nuclear magnetic resonance (NMR) fluid typing methods and correlations, Petroleum 2 (2016) 138–147.

[64] Y. Yuan, R. Rezaee, Impact of paramagnetic minerals on NMR-converted pore size distributions in Permian Carynginia shales, Energy & Fuels 33 (2019) 2880–2887.

[65] H. Y. Carr, E. M. Purcell, Effects of diffusion on free precession in nuclear magnetic resonance experiments, Physical review 94 (1954) 630.

[66] M. Dieterich, B. Kutchko, A. Goodman, Characterization of Marcellus Shale and Huntersville Chert before and after exposure to hydraulic frac-

turing fluid via feature relocation using field-emission scanning electron microscopy, Fuel 182 (2016) 227–235.

[67] Q. Li, A. D. Jew, A. Kohli, K. Maher, G. E. Brown Jr, J. R. Bargar, Thicknesses of Chemically Altered Zones in Shale Matrices Resulting from Interactions with Hydraulic Fracturing Fluid, Energy & Fuels 33 (2019) 6878–6889.

[68] A. N. Paukert Vankeuren, J. A. Hakala, K. Jarvis, J. E. Moore, Mineral reactions in shale gas reservoirs: barite scale formation from reusing produced water as hydraulic fracturing fluid, Environmental Science & Technology 51 (2017) 9391–9402.

[69] R. J. Herz-Thyhsen, J. P. Kaszuba, J. C. Dewey, Mineral dissolution and precipitation induced by hydraulic fracturing of a mudstone and a tight sandstone in the powder river basin, wyoming, usa, Applied Geochemistry (2020) 104636.

[70] J. Lu, P. J. Mickler, J.-P. Nicot, W. Choi, W. L. Esch, R. Darvari, Geochemical interactions of shale and brine in autoclave experiments—understanding mineral reactions during hydraulic fracturing of Marcellus and Eagle Ford Shales, AAPG Bulletin 101 (2017) 1567–1597.

[71] M. Xu, H. Dehghanpour, Advances in understanding wettability of gas shales, Energy & Fuels 28 (2014) 4362–4375.

[72] J. Matthiesen, T. Hassenkam, N. Bovet, K. N. Dalby, S. L. S. Stipp, Adsorbed organic material and its control on wettability, Energy & Fuels 31 (2017) 55–64.

[73] U. Kuila, M. Prasad, Specific surface area and pore-size distribution in clays and shales, Geophysical Prospecting 61 (2013) 341–362.

[74] J. Rouquerol, F. Rouquerol, P. Llewellyn, G. Maurin, K. S. Sing, Adsorption by powders and porous solids: principles, methodology and applications, Academic press, 2013.

[75] B. Feng, S. K. Bhatia, Variation of the pore structure of coal chars during gasification, Carbon 41 (2003) 507–523.

[76] J. C. Groen, L. A. Peffer, J. Perez-Ramirez, Pore size determination in modified micro-and mesoporous materials. pitfalls and limitations in gas adsorption data analysis, Microporous and mesoporous materials 60 (2003) 1–17.

[77] J. Poonoosamy, S. Haber-Pohlmeier, H. Deng, G. Deissmann, M. Klinkenberg, B. Gizatullin, S. Stapf, F. Brandt, D. Bosbach, A. Pohlmeier, Combination of MRI and SEM to Assess Changes in the Chemical Properties and Permeability of Porous Media due to Barite Precipitation, Minerals 10 (2020) 226.

[78] M. Saidian, L. J. Godinez, M. Prasad, Effect of clay and organic matter on nitrogen adsorption specific surface area and cation exchange capacity in shales (mudrocks), Journal of Natural Gas Science and Engineering 33 (2016) 1095–1106.